

Dynamics of surface water in ZrO_2 studied by quasielastic neutron scattering

E. Mamontov^{a)}

NIST Center for Neutron Research, National Institute of Standards and Technology, Gaithersburg, Maryland 20899-8562 and Department of Materials Science and Engineering, University of Maryland, College Park, Maryland 20742-2115

(Received 23 June 2004; accepted 16 August 2004)

A quasielastic neutron scattering experiment has revealed the dynamics of surface water in a high surface area zirconium oxide in the temperature range of 300–360 K. The characteristic times of the rotational (picoseconds) and translational (tens of picoseconds) components of diffusion motion are well separated. The rotational correlation time shows an Arrhenius-type behavior with an activation energy of 4.48 kJ/mol, which is lower compared to bulk water. The rotational diffusion at room temperature is slower by about a factor of 2 compared to bulk water, whereas the translational diffusion slows down by a factor of 40. In contrast to bulk water, the translational correlation time exhibits an Arrhenius-type temperature dependence with an activation energy of 11.38 kJ/mol. Comparison of different models for jump diffusion processes suggests that water molecules perform two-dimensional jumps at a well-defined, almost temperature-independent distance of 4.21–4.32 Å. Such a large jump distance indicates a low molecular density of the layer of diffusing molecules. We argue that undissociated water molecules on an average form two hydration layers on top of the surface layer of hydroxyl groups, and all the layers have similar molecular density. Quasielastic neutron scattering experiment assesses the dynamics of the outermost hydration layer, whereas slower motion of the water molecules in the inner hydration layer contributes to the elastic signal.

© 2004 American Institute of Physics. [DOI: 10.1063/1.1804152]

I. INTRODUCTION

Unless a dehydroxylation treatment is applied, water species are always present on an oxide surface. Chemisorbed surface hydroxyl groups saturate the coordination of surface cations and complete the interrupted bulk crystalline network. Under ambient conditions, water molecules are physisorbed on oxide surfaces. The influence of surface water on the oxide properties increases rapidly with the increase of the specific surface area as the ratio of surface-to-bulk atoms grows. In technologically important high surface area oxides having specific surface area of tens or hundreds meters squared per gram, adsorbed water exerts a great influence on the surface properties of the oxide.

The exceptionally large incoherent scattering cross section of hydrogen compared to other elements makes neutron scattering an attractive technique to study the dynamics of surface water. Quasielastic neutron scattering (QENS) is indispensable for studying the mobility of water molecules through the dependence of quasielastic scattering intensity on the scattering vector. As a method of choice, QENS has been used for a great variety of water-containing materials, both organic and inorganic.^{1–23} However, the dynamics of surface water in oxides has received almost no attention compared to water confined in porous glass such as vycor,^{9,12,17} mesoporous silica,¹⁵ MCM-41 (Refs. 16 and 23), or interlayer water in clays.^{2,4,5,19–21} A rare exception is the study of condensed surface water on hydroxylated Cr_2O_3 by

Kuroda *et al.*,²⁴ which demonstrated quasielastic broadening associated with the dynamics of a monolayer of water near room temperature. This relative absence of QENS data on surface water dynamics in high surface area oxides is surprising given their importance in catalysis. In this work, we report a QENS study of the mobility of surface water in a high surface area zirconium oxide ZrO_2 . Surface hydroxyl groups and undissociated water molecules play an important role in many reactions over zirconia, such as methanol synthesis and isosynthesis reaction of $\text{CO}/\text{H}_2/\text{H}_2\text{O}$.²⁵ In automotive catalysis, zirconia is an important additive to ceria, which is a catalyst for water-gas shift reaction $\text{CO} + \text{H}_2\text{O} \rightarrow \text{CO}_2 + \text{H}_2$. Furthermore, one can expect QENS measurements of surface water in ZrO_2 to reveal some general features of water dynamics on oxide surfaces.

To date, neutron scattering was employed to investigate vibrational dynamics of surface water in ZrO_2 .²⁶ The aim of the present work is to study the mobility of surface water in zirconia near and above room temperature, with the coverage formed under ambient conditions. This is a not a simple task in several aspects. To begin with, the single-particle dynamics of interfacial water molecules is not thoroughly understood. Only recently a coherent picture spanning both short and long time intervals of the diffusion relaxation process²⁷ and incorporating the coupling between translational and rotational molecular motions²⁸ has begun to emerge. Also, the surface structure of monoclinic zirconia, while exhibiting a preferred termination along the (111) plane,²⁹ is not very uniform, and water adsorption on zirconia surfaces in general does not show distinct steps of layer adsorption.^{30,31} Addi-

^{a)}Fax: (301) 921-9847. Electronic mail: mamontov@nist.gov

tionally, even though the incoherent neutron scattering cross section for both Zr and O is very small, the presence of surface hydroxyl groups gives rise to a strong elastic signal, which makes the accurate subtraction of it from the data problematic. Finally, the quasi-two-dimensional nature of water diffusion on the surface of randomly oriented crystallites further complicates data analysis compared to more commonly studied three-dimensional diffusion. Nevertheless, we demonstrate that by applying simple models for water diffusion which assume the decoupling of translational and rotational motions, one can successfully analyze QENS data and obtain meaningful results even for water on a non-uniform surface such as that of ZrO_2 crystallites. In particular, we find that the residence time for translational diffusion of surface water in ZrO_2 at room temperature increases by roughly a factor of 40 compared to bulk water, whereas the correlation time of rotational diffusion component increases just by a factor of 2. This effectively separates the characteristic times of rotational and translational diffusion components, which are comparable in bulk water at room temperature, thereby ensuring the validity of decoupling approximation for data analysis. In contrast to bulk water, the characteristic time of not only the rotational but also the translational motion displays an Arrhenius-type temperature dependence within the studied temperature range of 300–360 K. Having tried several models for translational diffusion, we found that the QENS data are best described by a quasi-two-dimensional jump diffusion process with a fixed jump length. Regardless of the model used, the data analysis yields very long jump distances which are incompatible with proton jumps across the tetrahedral angle of four-coordinated molecules known for bulk water.^{32,33} We argue that the outermost layer of the surface water in ZrO_2 differs from bulk water in many aspects. It has low molecular density, is bonded to the immobile (or slow moving) molecules of the inner hydration layer, and its translational mobility is due to thermally activated, Arrhenius-type surface jump diffusion.

II. EXPERIMENT

Zirconium oxide powder sample with a specific surface area of $80 \text{ m}^2/\text{g}$ was obtained from Magnesium Elektron Inc., New Jersey. The peak width analysis of the x-ray diffraction pattern obtained using a Bruker D8 powder diffractometer yielded a crystallite size of $\sim 150 \text{ \AA}$. As received powder was annealed in air at 873 K in order to ensure the removal of any organic residue from the surface. The IR measurements of the powder were performed at room temperature with a Thermo Nicolet Nexus 670 Fourier transform infrared (FTIR) spectrometer having a resolution of 4 cm^{-1} . The IR spectra indicated the presence of undissociated surface water. A hydroxylated monoclinic ZrO_2 surface free of undissociated water is characterized by two well-defined peaks at ~ 3780 and $\sim 3670 \text{ cm}^{-1}$ due to O-H stretch mode of terminal (coordinated to only one surface cation) and bridged (coordinated to three surface cations) hydroxyl groups, respectively.^{29,34} Instead, we observed a single broad peak at $\sim 3690 \text{ cm}^{-1}$, similar to the one assigned to a stretch O-H mode of molecularly adsorbed water on CeO_2 ,^{34,35} and a fingerprint molecular water feature at $\sim 1630 \text{ cm}^{-1}$ due to

H-O-H bending.³⁵ The thermal gravimetric analysis (TGA) measurements of the powder in the temperature range of 300–673 K showed a weight loss of 2.5%. The TGA measurements were repeated three times following the full recovery of the initial weight by the sample stored overnight under ambient conditions, and demonstrated reproducibility and reversibility of the weight loss. The FTIR spectra collected prior to the TGA measurements and after the sample regained its weight were practically identical. Because surface dehydroxylation is not expected under the conditions of the TGA measurements,²⁹ the reversible weight loss was attributed to undissociated water. This attribution allows one to calculate the molecular water content to be 0.17 mole per mole of ZrO_2 , corresponding to 10.5 water molecules per 100 \AA^2 of the surface. Water adsorption on zirconia surfaces in general does not show distinct steps associated with layer-by-layer adsorption.^{30,31} Nevertheless, one can estimate the average surface coverage by assuming that 4.6 H_2O molecules cover a fully hydroxylated surface of 100 \AA^2 , as found for OH species in silica,³⁶ yielding an average surface coverage of 2.3 layers. Alternatively, assuming an areal density of $\sim 11 \text{ H}_2\text{O}$ molecules per 100 \AA^2 based on the bulk water density, one would obtain the average surface coverage of one layer. As will be discussed in the following sections, the results we obtained are consistent with the presence of about two layers of molecular water on top of the surface hydroxyl groups.

QENS experiment was carried out using the cold neutron time-of-flight disk chopper spectrometer (DCS) (Ref. 37) at the National Institute of Standards and Technology Center for Neutron Research. Water-containing ZrO_2 powder was placed in a thin annular aluminum sample holder chosen to ensure greater than 90% neutron beam transmission through the sample, sealed with an indium O ring, and mounted onto a closed-cycle refrigerator. The temperature was controlled within $\pm 0.5 \text{ K}$. The incident neutron wavelength was $\lambda = 9.0 \text{ \AA}$ ($E_0 = 1.0 \text{ meV}$). At this incident energy, the high-intensity operation mode of the instrument provides an energy resolution of about 19 \mu eV (full width at half maximum), as measured with the sample at 60 K. The DCS detectors are located 4000 mm from the sample at scattering angles from 5° to 140° . Because of the overwhelmingly strong small-angle elastic scattering, the low-angle detectors were excluded from the data analysis. To improve the statistics for data analysis, the data from the 649 detectors covering the range of the scattering vectors $0.40 \text{ \AA}^{-1} < Q < 1.20 \text{ \AA}^{-1}$ (at the elastic channel) have been summed and rearranged to yield 11 spectra with constant energy binning of the data points for the energy range of $\pm 500 \text{ \mu eV}$.

Following the collection of QENS spectra at 300, 320, 340, and 360 K, the data were measured at 60 K to obtain the instrument resolution function. Then the indium seal was removed and the sample was evacuated *in situ* for 1 h at $T = 375 \text{ K}$ to about 10^{-5} Torr using a turbo pump. The final set of data was then collected at $T = 300 \text{ K}$ from the evacuated sample. Such a treatment is expected to remove the physisorbed water species without affecting chemisorbed hydroxyl groups. As can be seen in Fig. 1, the evacuation at 375 K eliminates virtually all of the quasielastic scattering,

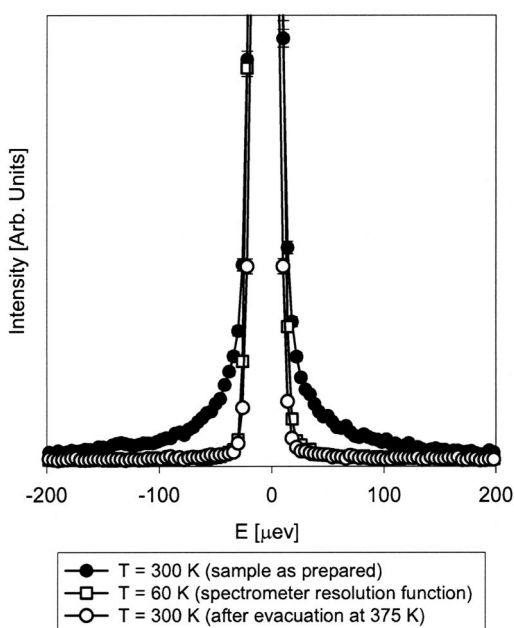


FIG. 1. The effect of evacuation on the neutron spectrum of surface water in ZrO_2 collected at $Q = 1.04 \text{ \AA}^{-1}$. The energy transfer range and the elastic peak are truncated. Mobile water that gives rise to the quasielastic wings is removed by the evacuation treatment at 375 K. The resulting completely elastic peak is similar in width to the instrument resolution function.

resulting in a completely elastic spectrum whose shape is quite similar to the measured instrument resolution function. This reassures us that the observed QENS signal is due to surface water rather than water species confined in closed pores that would not be desorbed in the course of evacuation treatment.

III. RESULTS AND ANALYSIS

Figures 2 and 3 show the temperature dependence of the scattering intensity collected at $Q = 1.04 \text{ \AA}^{-1}$. Similar to spectra obtained from bulk water, the QENS signal exhibits a broad and a narrow component. The former is visible when the whole range of measured energy transfers, $-500 \mu\text{eV} < E < 500 \mu\text{eV}$, is plotted (Fig. 2), whereas the latter can be visualized when the central region is expanded [Figs. 3(a) and 3(b)]. As will be discussed below, the broad component ascribed to rotational diffusion was modeled using a sum of Lorentzians. Different types of QENS broadening, both Lorentzian [Fig. 3(a)] and more peaked non-Lorentzian [Fig. 3(b)] were tried for modeling of the narrow component originated from translational diffusion. The general trend is that the width of the quasielastic signal grows as the temperature is increased, which demonstrates faster diffusion at higher temperatures. In addition to the QENS signal from mobile water species, the spectra include a strong elastic line owing to the scattering from zirconia crystallites, surface hydroxyl groups, and, possibly, water molecules which are immobile on the time scale of the experiment. One expects that most of the coherent scattering from zirconia is localized in the Bragg peaks and the low- Q region, where the small-angle scattering intensity from a high surface area powder is expected to grow rapidly. This, in combination with the very

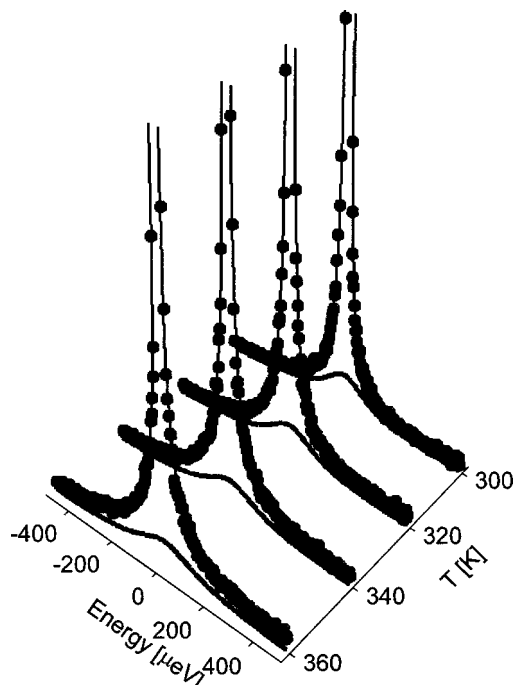


FIG. 2. The QENS data collected at $Q = 1.04 \text{ \AA}^{-1}$ (filled symbols), the overall fit obtained using the model for two-dimensional diffusion with a fixed jump length (solid line), and the quasielastic contribution due to the rotational diffusion component (bold line). The elastic peak is truncated.

small incoherent scattering cross section for zirconium and oxygen and the relatively large fraction of water molecules in the sample (0.17 molecules of removable water species per 1 molecule of ZrO_2 in addition to nonremovable OH groups) suggests that the scattering contribution from zirconia itself is negligible, except for the low- Q region and the scattering vectors corresponding to ZrO_2 Bragg peaks. While the elastic scattering from a matrix or substrate is often subtracted from the measured data, we chose not to perform such a subtraction because determining the fraction of “immobile” OH/ H_2O species on the time scale of the experiment versus mobile H_2O molecules is difficult. Instead, we fitted the data using the following expression:

$$I(Q, E) = A(Q) \{ x(Q) \delta(E) + [1 - x(Q)] S(Q, E) \} + BE + C \quad (1)$$

convolved with the spectrometer resolution function. Here A is a scaling constant, x is the fraction of the elastic scattering, $S(Q, E)$ is a model quasielastic scattering function, and the terms BE and C describe the inelastic background. While various forms of $S(Q, E)$ were tried, none of them contained a purely elastic term (as would be the case for purely rotational diffusion) because a nonlocal translational diffusion process was always incorporated into the model scattering function. The values of $x(Q)$ obtained with different $S(Q, E)$ were very similar, with the difference less than 3% at any Q point. Figure 4 shows the fraction of the elastic scattering obtained using the best fit model for $S(Q, E)$ which will be discussed below. The upper Q limit of the QENS data range was just below the first Bragg peak of monoclinic ZrO_2 , a very weak (100) peak at $Q = 1.23 \text{ \AA}^{-1}$. The presence of this peak increased $x(Q)$ very little. At low Q , a substantial rise

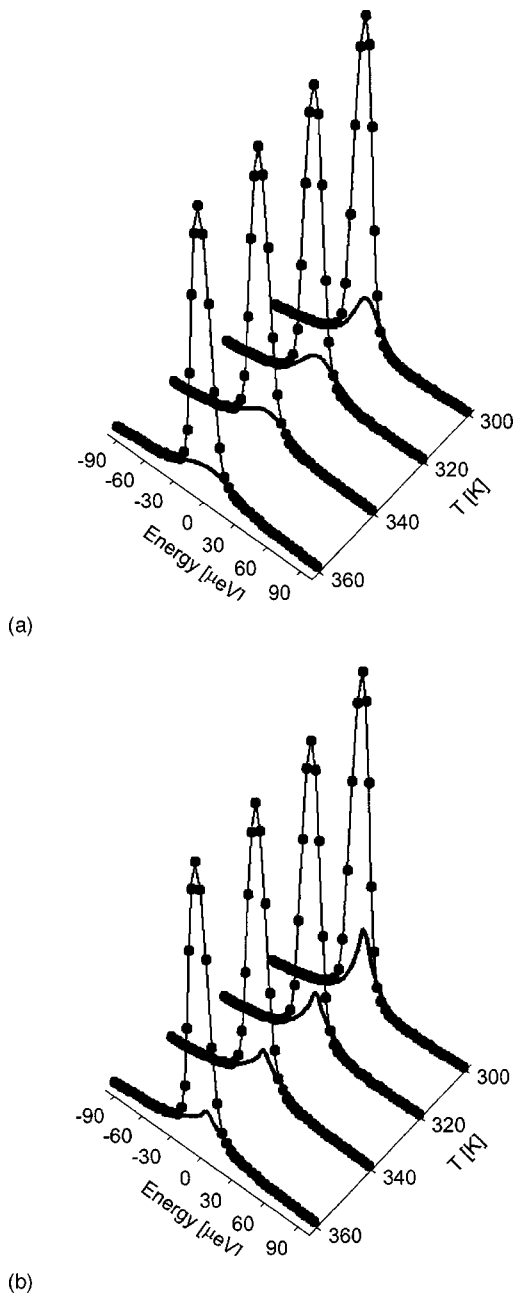


FIG. 3. Near elastic peak region of the QENS data collected at $Q = 1.04 \text{ \AA}^{-1}$ (filled symbols) fitted with (a) the model for three-dimensional diffusion (Lorentzian) and (b) the model for two-dimensional diffusion with a fixed jump length. The overall fit and the quasielastic contribution due to translational diffusion component are shown with solid and bold lines, respectively.

in $x(Q)$ was observed. This rise originated from small-angle scattering, as evident from the comparison of the fraction of the elastic scattering with the x-ray diffraction intensity in Fig. 4. In fact, as mentioned in the preceding section, very strong elastic small-angle scattering signal imposed a lower limit on the useful data range, forcing us to exclude low- Q detectors from the analysis.

Assuming that the rotational and translational motions of the water molecules can be treated as independent in time and space, one can write the intermediate scattering function as

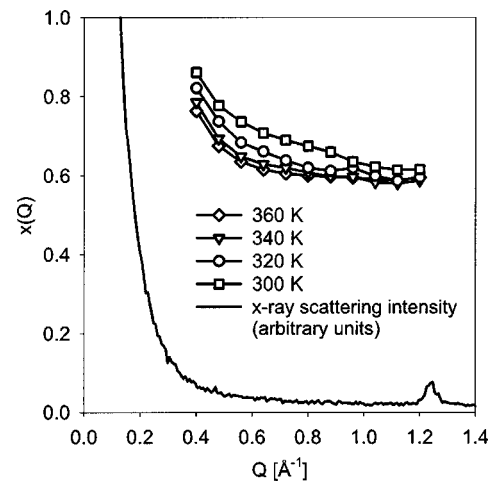


FIG. 4. The fraction of the elastic scattering [$x(Q)$ in Eq. (1)]. X-ray data are shown to illustrate the small-angle scattering (not to scale).

$$F(Q, t) = R(Q, t)T(Q, t), \quad (2)$$

where $R(Q, t)$ and $T(Q, t)$ represent the rotational and translational components of the motion. The scattering function can then be written as

$$S(Q, E) = R(Q, E) \otimes T(Q, E). \quad (3)$$

The convolution in energy is facilitated by the fact that the intermediate scattering functions that we use consist of only time-independent and exponential terms:

$$R(Q, t) = j_0^2(Qa) + 3j_1^2(Qa) \exp[-t/(3\tau_R)] + 5j_2^2(Qa) \exp[-t/\tau_R] \quad (4)$$

for rotational diffusion with correlation time τ_R and (in the simplest case)

$$T(Q, t) = \exp\left[-\Gamma(Q) \frac{t}{\hbar}\right] \quad (5)$$

for translational diffusion. Equation (4) represents the first three terms of the expansion due to Sears³⁸ for rotational diffusion of a molecule. For a water molecule, a is the O-H distance which is 0.98 \AA . Then for the Q range of our measurements, $Q < 1.20 \text{ \AA}^{-1}$, only the first three terms in the expansion (4) of the corresponding infinite series make non-negligible contribution to $R(Q, t)$. Then the Fourier transformation of Eqs. (4) and (5) yields

$$R(Q, E) = j_0^2(Qa) \delta(E) + 3j_1^2(Qa) \frac{1}{\pi} \frac{\hbar/(3\tau_R)}{E^2 + [\hbar/(3\tau_R)]^2} + 5j_2^2(Qa) \frac{1}{\pi} \frac{\hbar/\tau_R}{E^2 + [\hbar/\tau_R]^2}, \quad (6)$$

$$T(Q, E) = \frac{1}{\pi} \frac{\Gamma(Q)}{E^2 + \Gamma^2(Q)}. \quad (7)$$

The parameter $\Gamma(Q)$ represents the half width at half maximum (HWHM) of the Lorentzian quasielastic broadening associated with translational diffusion. For the total intermediate scattering function

TABLE I. Parameters obtained from fitting the Q dependence of the Lorentzian half width at half maximum presented in Fig. 5. The mean jump length was calculated from the fit parameters τ_T and D_{3D} as $(\langle r^2 \rangle)^{1/2} = (D_{3D}6\tau_T)^{1/2}$.

T (K)	$\tau_R (\times 10^{-12}$ s)	3D, fixed jump length			3D, Gaussian jump length distribution		
		$\tau_T (\times 10^{-12}$ s)	$(\langle r^2 \rangle)^{1/2}$ (Å)	$D_{3D} (\times 10^{-10}$ m ² /s)	$\tau_T (\times 10^{-12}$ s)	$(\langle r^2 \rangle)^{1/2}$ (Å)	$D_{3D} (\times 10^{-10}$ m ² /s)
360	1.52	19.14	5.29	24.4	16.78	5.88	34.4
340	1.64	23.52	5.15	18.8	20.38	5.72	26.8
320	1.83	30.43	5.25	15.1	26.68	6.14	23.6
300	2.04	40.81	5.48	12.2	36.66	6.85	21.3

$$\begin{aligned}
 F(Q,t) = & j_0^2(Qa) \exp\left[-\Gamma(Q) \frac{t}{\hbar}\right] \\
 & + 3j_1^2(Qa) \exp\left[-t/(3\tau_R) - \Gamma(Q) \frac{t}{\hbar}\right] \\
 & + 5j_2^2(Qa) \exp\left[-t/\tau_R - \Gamma(Q) \frac{t}{\hbar}\right]. \quad (8)
 \end{aligned}$$

Therefore, the total scattering function in the energy space can be represented as

$$\begin{aligned}
 S(Q,E) = & j_0^2(Qa) \frac{1}{\pi} \frac{\Gamma(Q)}{E^2 + \Gamma^2(Q)} \\
 & + 3j_1^2(Qa) \frac{1}{\pi} \frac{[\hbar/(3\tau_R) + \Gamma(Q)]}{E^2 + [\hbar/(3\tau_R) + \Gamma(Q)]^2} \\
 & + 5j_2^2(Qa) \frac{1}{\pi} \frac{[\hbar/\tau_R + \Gamma(Q)]}{E^2 + [\hbar/\tau_R + \Gamma(Q)]^2}. \quad (9)
 \end{aligned}$$

The characteristic time for rotational diffusion is often much shorter compared to translational diffusion. Equation (9) then comprises broad components originating mainly from faster rotational diffusion and a narrow component due to slower translational diffusion.

The analysis of the quasielastic spectra using Eqs. (1) and (9) with a fixed value of $a = 0.98$ Å yielded the rotational diffusion correlation times τ_R listed in Table I, and the half width at half maximum $\Gamma(Q)$, as plotted in Fig. 5. The overall trend is that the $\Gamma(Q)$ broadens as temperature is increased, indicating a faster translational diffusion. The Q dependence of the broadening seems to exhibit a weak maximum at intermediate Q values, which becomes somewhat more pronounced at higher temperatures. The presence or absence of such a maximum is crucial in determining the nature of the jump diffusion process. The presence of a maximum is a fingerprint of a jump diffusion process with a fixed jump length L_0 . For a three-dimensional jump diffusion process with the residence time τ_T between jumps, the scattering function averaged over the angular coordinates of the vector Q is a Lorentzian with the half width at half maximum,

$$\Gamma(Q) = \frac{\hbar}{\tau_T} \left(1 - \frac{\sin(QL_0)}{QL_0}\right) = \frac{\hbar}{\tau_T} [1 - j_0(QL_0)], \quad (10)$$

where j_0 is the spherical Bessel function of zeroth order.³⁹ The residence time and jump length are related through the

three-dimensional diffusion coefficient $D_{3D} = L_0^2/6\tau_T$. For a distribution of jump lengths $P_{3D}(r)$, the HWHM further averaged over the jump lengths becomes

$$\Gamma(Q) = \frac{\hbar}{\tau_T} \frac{\int_0^\infty \left(1 - \frac{\sin Qr}{Qr}\right) P_{3D}(r) dr}{\int_0^\infty P_{3D}(r) dr}. \quad (11)$$

The choice of $P_{3D}(r)$, which is not unique, defines the Q dependence of the HWHM. For a Gaussian distribution of jump lengths in three dimensions,

$$P_{3D}(\mathbf{r}) = \frac{1}{r_0^3 \sqrt{(2\pi)^3}} \exp(-\mathbf{r}^2/2r_0^2), \quad (12)$$

which corresponds to the normalized scalar distribution of jump lengths

$$P_{3D}(r) = \frac{2r^2}{r_0^3 \sqrt{2\pi}} \exp(-r^2/2r_0^2) \quad (13)$$

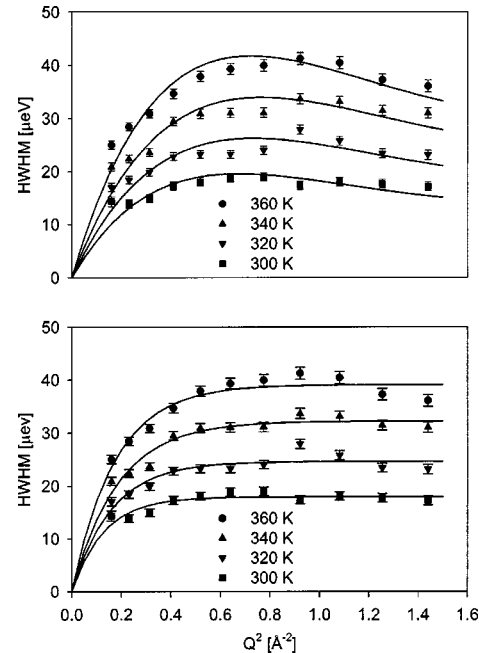


FIG. 5. Q dependence of the Lorentzian half width at half maximum obtained assuming three-dimensional diffusion, and its fitting with translational jump diffusion models with a fixed jump length (top) and a Gaussian distribution of jump lengths (bottom).

with mean square jump length $\langle r^2 \rangle = 3r_0^2$, the half width at half maximum as derived by Hall and Ross⁴⁰ is

$$\begin{aligned}\Gamma(Q) &= \frac{\hbar}{\tau_T} [1 - \exp(-Q^2 r_0^2/2)] \\ &= \frac{\hbar}{\tau_T} [1 - \exp(-D_{3D} Q^2 \tau_T)],\end{aligned}\quad (14)$$

where the three-dimensional diffusion coefficient $D_{3D} = \langle r^2 \rangle / 6\tau_T$. Alternatively, an exponential distribution of jump lengths^{39,41} can be used that results in $\Gamma(Q)$ different from Eq. (14). We chose a Gaussian distribution since it has been employed successfully to describe translational dynamics of interfacial water^{4,20,21} and allows easy generalization for two-dimensional geometry. In both Eqs. (10) and (14), the Q dependence shows the correct asymptotic behavior, $\Gamma(Q \rightarrow 0) = \hbar D_{3D} Q^2$ and $\Gamma(Q \rightarrow \infty) = \hbar / \tau_T$, but, unlike Eq. (10), Eq. (14) does not exhibit a maximum at intermediate values of Q .

As listed in Table I, both the fixed jump length model and the model with a Gaussian distribution of jump lengths yielded rather similar values for τ_T , while the differences in the values for the diffusion coefficient were somewhat larger. It should be noted that for the translational diffusion the jump lengths are considerably larger than for bulk water, while τ_T is much longer. These combine to give a diffusion coefficient that is a fraction of that for bulk water.

In order to assess the confidence we can place on the model parameters, and to make a decisive conclusion on the nature of the jump diffusion (a fixed jump length versus a distribution of jump lengths) we have to use a more realistic model that takes into consideration a quasi-two-dimensional character of the diffusion of surface water. Theory of QENS from species performing translational diffusion on a two dimensional surface has been developed by several authors.^{1,42,43} For diffusion in a plane with a fixed diffusion jump length L_0 and residence time τ_T between jumps, the scattering function averaged over the in-plane angular coordinate of the projection of the vector \mathbf{Q} on the plane of diffusion is still a Lorentzian with the HWHM,

$$\Gamma(Q) = \frac{\hbar}{\tau_T} [1 - J_0(QL_0 \sin \theta)],\quad (15)$$

where the cylindrical Bessel function of zeroth order, J_0 replaces the spherical Bessel function in Eq. (10).^{43,44} Here θ is the angle between the normal direction to the plane and the direction of vector \mathbf{Q} . However, for an array of randomly oriented diffusion planes, the scattering function has to be further averaged over θ . The resulting translational component of the scattering function is no longer a simple Lorentzian:^{43,44}

$$T(Q, E) = \frac{1}{2} \int_0^\pi \sin \theta d\theta \frac{1}{\pi} \frac{\frac{\hbar}{\tau_T} [1 - J_0(QL_0 \sin \theta)]}{E^2 + \left[\frac{\hbar}{\tau_T} [1 - J_0(QL_0 \sin \theta)] \right]^2}.\quad (16)$$

Equation (16) diverges when both $E, \theta \rightarrow 0$ (that is, when \mathbf{Q} is perpendicular to the diffusion plane, and diffusion has no influence on the scattering anymore). The singularity in the scattering law is not seen experimentally because of a finite instrument energy resolution, and a scattering function more peaked compared to a Lorentzian is observed instead. For $QL_0 \ll 1$, expansion $J_0(x) = 1 - x^2/4 + \dots$ yields

$$T(Q, E) = \frac{1}{2} \int_0^\pi \sin \theta d\theta \frac{1}{\pi} \frac{\hbar D_{2D} Q^2 \sin^2 \theta}{E^2 + (\hbar D_{2D} Q^2 \sin^2 \theta)^2},\quad (17)$$

where the two-dimensional diffusion coefficient $D_{2D} = L_0^2 / 4\tau_T$. Equation (17) is often used if one is mainly concerned with determining macroscopic surface diffusion coefficient from low- Q data.⁴⁵⁻⁴⁸ For this case, the problem of a singularity in the data has been treated by Lechner.⁴⁹ More complex model scattering functions have been developed to analyze the data that exhibit a maximum in $\Gamma(Q)$ on the basis of models for diffusion with a fixed jump length, whether distributed in the plane,⁴⁴ or localized on a two-dimensional lattice.⁵⁰ For a fixed jump length in a plane, L_0 the translational scattering function (16) exhibits a maximum at intermediate Q values similar to Eq. (10). To properly analyze the diffusion process with a distribution of jump lengths, which would lead to a monotonic increase of $\Gamma(Q)$ similar to Eq. (14), we are forced to use even more complex model for the translational scattering function

$$\begin{aligned}T(Q, E) &= \frac{1}{2} \int_0^\pi \sin \theta d\theta \frac{1}{\pi} \\ &\quad \times \frac{\frac{\hbar}{\tau_T} \int_0^\infty [1 - J_0(Qr \sin \theta)] P_{2D}(r) dr}{E^2 + \left[\frac{\hbar}{\tau_T} \int_0^\infty [1 - J_0(Qr \sin \theta)] P_{2D}(r) dr \right]^2}.\end{aligned}\quad (18)$$

The normalized two-dimensional expression analogous to Eq. (12),

$$P_{2D}(\mathbf{r}) = \frac{1}{2\pi r_0^2} \exp(-\mathbf{r}^2/2r_0^2)\quad (19)$$

corresponds to the normalized scalar distribution of jump lengths

$$P_{2D}(r) = \frac{r}{r_0^2} \exp(-r^2/2r_0^2)\quad (20)$$

with mean square jump length $\langle r^2 \rangle = 2r_0^2$. The mean square jump length and residence time are related through the two-dimensional diffusion coefficient $D_{2D} = \langle r^2 \rangle / 4\tau_T$.

Figure 6 illustrates the difference between the scattering functions $T(Q, E)$ for three- and two-dimensional diffusion calculated at $Q = 1.0 \text{ \AA}^{-1}$ for arbitrarily chosen parameters $\tau_T = 10 \text{ ps}$ and $L_0 = 3 \text{ \AA}$ [or $(\langle r^2 \rangle)^{1/2} = 3 \text{ \AA}$, that is, $r_0 = 3 \times (2)^{-1/2} \text{ \AA}$ in Eq. (20)]. Both two-dimensional diffusion processes yield more peaked scattering functions compared to the Lorentzian resulting from a three-dimensional diffusion process with similar parameters. Between the two-

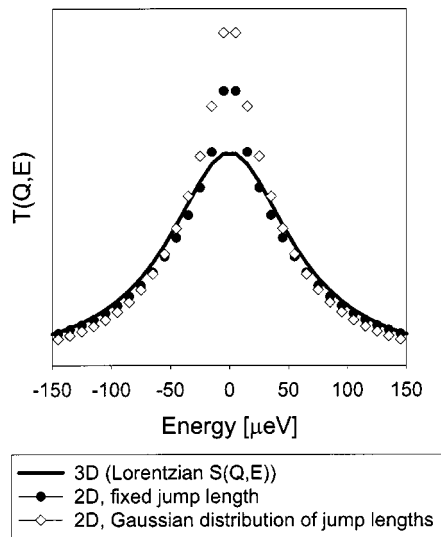


FIG. 6. An illustration of the effect of two-dimensionality on the translational component of the scattering function calculated at $Q = 1.0 \text{ \AA}^{-1}$ for the residence time of 10 ps and the jump length (or average jump length) of 3 Å.

dimensional processes, the one with a Gaussian jump length distribution produces a more peaked scattering function owing to the presence of some very short distances in the jump length distribution.

The procedure for obtaining the two-dimensional diffusion parameters from the experimental data is different from the one described above for the three-dimensional diffusion process. In the latter case, the shape of the QENS signal (a Lorentzian) is known *a priori*. The HWHM of the Lorentzians are obtained at each Q point, and the resulting $\Gamma(Q)$ is fitted with an expression such as Eq. (10) or Eq. (14) that includes diffusion parameters as fitting variables. For two-dimensional jump diffusion, the theoretical scattering function is no longer a Lorentzian. Thus, τ_T and L_0 [or r_0 if Eqs. (18) and (20) are used] should be obtained at each Q point independently by means of fitting the experimental data using the total scattering function which is similar to Eq. (9) but incorporates a proper averaging for a two-dimensional process:

$$\begin{aligned}
 S(Q, E) = & j_0^2(Qa) \frac{1}{2} \int_0^\pi \sin \theta d\theta \frac{1}{\pi} \frac{\Gamma(Q, \sin \theta)}{E^2 + [\Gamma(Q, \sin \theta)]^2} \\
 & + 3j_1^2(Qa) \frac{1}{2} \int_0^\pi \sin \theta d\theta \\
 & \times \frac{1}{\pi} \frac{\Gamma(Q, \sin \theta) + (\hbar/3\tau_R)}{E^2 + [\Gamma(Q, \sin \theta) + (\hbar/3\tau_R)]^2} \\
 & + 5j_2^2(Qa) \frac{1}{2} \int_0^\pi \sin \theta d\theta \\
 & \times \frac{1}{\pi} \frac{\Gamma(Q, \sin \theta) + (\hbar/\tau_R)}{E^2 + [\Gamma(Q, \sin \theta) + (\hbar/\tau_R)]^2}, \quad (21)
 \end{aligned}$$

where $\Gamma(Q, \sin \theta)$ is defined by Eq. (15) for a fixed jump length diffusion and

$$\Gamma(Q, \sin \theta) = \frac{\hbar}{\tau_T} \int_0^\infty [1 - J_0(Qr \sin \theta)] P_{2D}(r) dr \quad (22)$$

for the distribution of jump lengths described by Eq. (20). The values for the translational diffusion time and jump distance obtained in the fitting procedure should be averaged over all Q points. In the simple case of three-dimensional diffusion giving rise to a Lorentzian broadening, the same effective averaging of the model parameters over Q is achieved in the course of fitting all Q points in $\Gamma(Q)$ with a single function depending on diffusion parameters.

To restrict the number of fitting parameters, we used the rotational diffusion time τ_R obtained in the modeling for a three-dimensional diffusion as listed in Table I. Furthermore, it is easy to see that the residence time between jumps is independent of averaging over jump distances and orientations in Eqs. (21) and (22). Therefore, for the two-dimensional processes with a fixed jump length and a jump length distribution we used the values of τ_T obtained previously for the three-dimensional diffusion processes with the corresponding model for jump length as listed in Table I. Indeed, applying a two-dimensional rather than a three-dimensional model should have an effect on the parameters describing the jump length, but not the residence time between jumps. In the system we studied, further simplification of the model is possible in principle because τ_R is much smaller than τ_T . This makes the portion of $S(Q, E)$ in Eq. (21) that fits the narrow translational diffusion component predominantly sensitive to the first term and largely independent of the next terms, which are much broader. It should be noted that the fact that the first term in Eq. (21) is independent of τ_R justifies fixing the rotational diffusion time. Besides, the last term in Eq. (21) proportional to $j_2^2(Qa)$ remains small because of the limited Q range, which allows further simplification of the model scattering function. On the other hand, for systems with smaller separation between translational and rotational characteristic times using all terms in Eq. (21) is essential. In our analysis, we used non-simplified Eq. (21).

To assess the quality of models, we compared the agreement factors obtained using Eq. (9) (Model I), Eqs. (21) and (15) (Model II), and Eqs. (21) and (22) (Model III) at each Q point. The results are summarized in Table II. Except for two points in 300 K data set, the best agreement is always obtained using Eqs. (21) and (15), whereas the scattering function described by Eqs. (21) and (22) typically yields second best agreement. This indicates that the translational component of water diffusion in the system we studied is indeed described by a quasi-two-dimensional jump diffusion process. Furthermore, this jump diffusion process is characterized by a fairly well-defined jump length rather than a distribution of jump lengths.

The diffusion parameters obtained with the best fit model using Eqs. (21) and (15) are summarized in Table III. Note the decrease of the jump distances compared to those obtained for the corresponding three-dimensional case as listed in Table I. This is because the position of the maximum in the QENS broadening as a function of Q for fixed jump length models is defined by the first minimum of the

TABLE II. The agreement factor $\chi^2 = \sum(I_{\text{experiment}} - I_{\text{model}})^2 / (N_{\text{observations}} - N_{\text{parameters}})$ obtained using different models for translational diffusion component: three-dimensional diffusion (I), two-dimensional diffusion with a fixed jump length (II), and two-dimensional diffusion with a Gaussian distribution of the jump lengths (III).

Q (\AA^{-1})	300 K			320 K			340 K			360 K		
	I	II	III									
0.40	0.534	0.518	0.524	0.679	0.641	0.651	0.686	0.642	0.651	0.784	0.715	0.730
0.48	0.692	0.668	0.676	0.822	0.768	0.784	0.809	0.748	0.763	0.882	0.777	0.806
0.56	0.926	0.895	0.909	0.954	0.885	0.910	1.074	0.992	1.015	1.052	0.941	0.979
0.64	0.928	0.905	0.923	1.040	0.984	1.018	1.050	0.974	1.016	1.023	0.923	0.973
0.72	0.734	0.687	0.727	0.658	0.586	0.631	0.682	0.604	0.658	0.685	0.594	0.661
0.80	0.606	0.570	0.612	0.561	0.497	0.537	0.651	0.569	0.626	0.664	0.573	0.654
0.88	0.598	0.585	0.615	0.639	0.587	0.626	0.776	0.691	0.750	0.722	0.630	0.718
0.96	0.785	0.759	0.777	0.888	0.839	0.968	0.946	0.873	0.956	0.971	0.888	0.987
1.04	0.992	0.973	0.992	0.998	0.938	1.004	1.029	0.932	1.023	0.780	0.689	0.780
1.12	0.755	0.760	0.757	0.646	0.594	0.625	0.566	0.498	0.547	0.622	0.526	0.587
1.20	0.604	0.629	0.609	0.565	0.545	0.555	0.499	0.443	0.480	0.556	0.469	0.516

spherical or cylindrical Bessel functions of the zeroth order, that is, $j_0(QL_0)$ for three-dimensional jump diffusion and $J_0(QL_0)$ for two-dimensional jump diffusion. Thus, $QL_0 \approx 4.5$ and $QL_0 \approx 4$ for the position of the maximum broadening for three- and two-dimensional case, respectively.

IV. DISCUSSION

Neglecting a presumably small contribution from zirconium and oxygen atoms outside the low- Q region, we can conclude from Fig. 4 that about 60% of hydrogen atoms in the sample are immobile on the measurement time scale. Assuming that all the H_2O molecules in the system are mobile and all the OH groups are immobile, one obtains that 25% of hydrogen-containing species in the sample are undissociated water molecules. This is way too small to account for the weight loss due to molecular water desorption, even if one takes the same areal density for hydroxyl groups and undissociated water molecules on top of them. This observation suggests that in addition to the surface OH groups a fraction of H_2O species is either immobile or moving too slowly for the instrument resolution, thus contributing to the elastic scattering. Such a separation into a fast and a slow component has been observed for interfacial water diffusion. For example, in a fully hydrated Na-vermiculite the dynamics of the “free” water molecules that are in contact only with other water molecules is faster by more than an order of magnitude compared to that of the molecules interacting with the surface and/or the intercalated ions.^{20,21} The scattering from the latter molecules was seen as an elastic line on the time scale of a time-of-flight spectrometer with 15 μeV

resolution.²⁰ Similarly, we may assume that the mobile water species that give rise to the QENS signal comprise water molecules in the outermost hydration layer, while those in direct contact with the hydroxylated surface are seen as immobile. Assuming the presence of two layers of molecular water with the areal density similar to that of surface hydroxyl groups, the outer layer with the dynamics observable in our 19 μeV resolution experiment and the inner one seen as immobile, one obtains the fraction of the elastic scattering [x in Eq. (1)] of 0.60 from the equal number of “fast” H_2O molecules, “slow” H_2O molecules, and surface OH groups. The presence of two layers of molecular water is in a good agreement with the weight loss measurements as discussed in the Experiment. It should be also noted that x in Fig. 4 decreases with temperature owing to growing number of water molecules contributing to the fast dynamics. It is possible that as temperature is increased, some slow water molecules loose the direct contact with the hydroxylated surface to join the network of fast water molecules.

An observation that a single layer of water on a hydroxylated surface of Cr_2O_3 exhibits a substantially slower dynamics than we observed²⁴ makes an additional supporting argument for the hypothesis that we assessed the dynamics of the free water molecules in the outermost hydration level. The HWHM of the broadening due to rotational motion in a single water layer in contact with hydroxylated surface of Cr_2O_3 was found to be ~ 20 μeV , which corresponds to a correlation time of about 10 ps versus 2 ps for our system at similar temperature.

We will now compare the dynamics of “free” surface water in ZrO_2 to that of bulk water. In the classical picture of bulk water at and below room temperature derived from QENS data,^{32,33,51} the decoupling between rotational and translational motions is postulated. The network of hydrogen bonds is very dense, and a water molecule is normally tetrahedrally coordinated. Breaking a hydrogen bond results in a hindered rotationlike motion, and the characteristic time of this process τ_R shows an Arrhenius-type temperature dependence with an activation energy of 7.74 kJ/mol.³³ When at least three bonds are simultaneously broken, translational diffusion is possible.⁵¹ The temperature dependence of the

TABLE III. Parameters obtained from the best fit using the two-dimensional jump diffusion model with a fixed jump length for the translational diffusion component. The diffusion coefficient was calculated from the fit parameters τ_T and $\langle r^2 \rangle$ as $D_{2D} = \langle r^2 \rangle / 4\tau_T$.

T (K)	$\tau_R (\times 10^{-12} \text{ s})$	$\tau_T (\times 10^{-12} \text{ s})$	$(\langle r^2 \rangle)^{1/2} (\text{\AA})$	$D_{2D} (\times 10^{-10} \text{ m}^2/\text{s})$
360	1.52	19.14	4.32	24.4
340	1.64	23.52	4.25	19.2
320	1.83	30.43	4.23	14.7
300	2.04	40.81	4.21	10.9

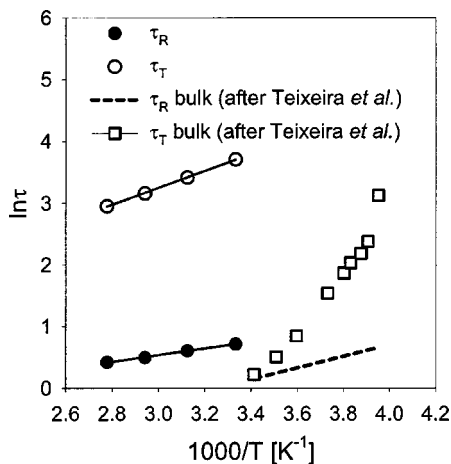


FIG. 7. Temperature dependence of the residence time for translational and rotational diffusion of surface water in ZrO_2 . The data for bulk water (after Teixeira *et al.*, Ref. 33) are shown for comparison.

correlation time for such a motion τ_T is non-Arrhenius. The jump distance associated with this mechanism becomes smaller as temperature is increased, which is explained in terms of the random network of water molecules.⁵² For a tetrahedrally coordinated water molecule, the diffusion involves a jump across the tetrahedral angle equal to 1.6 Å. At higher temperatures, the distribution of hydrogen bonds is more deformed making jumps at distances shorter than 1.6 Å possible.

Figure 7 shows the temperature dependence of the characteristic times for the rotational and translational components of water diffusion on ZrO_2 surface as listed in Table III along with the data for bulk water from Ref. 33. The rotational correlation time exhibits an Arrhenius-type behavior, $\tau_R = (0.341 \text{ ps}) \exp(E_A/RT)$, with the activation energy $E_A = 4.48 \text{ kJ/mol}$, which is lower than $E_A = 7.74 \text{ kJ/mol}$ for bulk water. At room temperature, the rotational diffusion of surface water molecules is slower compared to that of bulk water by about a factor of 2. Unlike the translational motion in bulk water, the temperature dependence of τ_T for surface water is very well described by an Arrhenius-type equation, $\tau_T = (0.424 \text{ ps}) \exp(E_A/RT)$, with the activation energy $E_A = 11.38 \text{ kJ/mol}$. This value is still much lower than that for the chemisorbed water species. For instance, rather high activation energy of 23.8 kJ/mol was measured for the mobility of surface OH species in ceria.⁵³ The residence time for the translational diffusion of surface water increases dramatically, being about 40 times longer compared to bulk water. Nevertheless, the translational diffusion coefficient is almost half the value for bulk water. For example, for bulk water $D(298 \text{ K}) = 22.99 \times 10^{-10} \text{ m}^2/\text{s}$ and $D(318 \text{ K}) = 35.75 \times 10^{-10} \text{ m}^2/\text{s}$,⁵⁴ whereas we obtained $D(300 \text{ K}) = 10.9 \times 10^{-10} \text{ m}^2/\text{s}$ and $D(320 \text{ K}) = 14.7 \times 10^{-10} \text{ m}^2/\text{s}$.

Large diffusion coefficients are the result of much larger jump distances compared to bulk water. For instance, $(\langle r^2 \rangle)^{1/2} = 1.29 \text{ Å}$ at $T = 293 \text{ K}$,³³ whereas in this study we found $(\langle r^2 \rangle)^{1/2} = 4.21 \text{ Å}$ at $T = 300 \text{ K}$. The jump length shows very weak temperature dependence, increasing slightly with temperature, and its magnitude rules out a jump across the tetrahedral angle as a diffusion mechanism. In any

scenario, such a large jump length is difficult to reconcile with the bulklike molecular density. Note also that the jump length does not seem to be directly associated with Zr-Zr nearest neighbor distances on (111) ZrO_2 surface. Assuming unmodified surface structure in the (111) termination plane of the monoclinic zirconia, one calculates Zr-Zr distances ranging from 3.12 to 4.33 Å, with an average of 3.71 Å. A large, nearly temperature-independent jump distance of 4.21–4.32 Å exceeds characteristic Zr-Zr nearest neighbor distance in the (111) plane, and should be correlated instead with the arrangement of the water molecules in the inner hydration layer. From a typical coverage of 4.6 molecules per 100 Å^2 as known for a fully hydroxylated surface of silica,³⁶ one can deduce a distance of 4.66 Å between hydroxyl groups in direct contact with the surface. As we have discussed, the assumption of two layers of molecular water with the areal density similar to that of surface hydroxyl groups yields a good agreement with the weight loss measurements and the observed fraction of the elastic scattering. In this scenario, the intermolecular distance in the hydration layers is rather similar to the jump length we observed.

Diffusion jump distances larger than those in bulk water have been reported previously. For water in fully hydrated phycocyanin⁶ and half hydrated Vycor glass,⁹ the translation diffusion coefficient similar to that of bulk water has been derived, despite the residence time between jumps being about four times longer. This implies a jump length twice larger than in bulk water at similar temperatures. These examples are qualitatively different from our system because of the water confinement in three dimensions. In both phycocyanin and Vycor, the translational diffusion within highly confined space gives rise to a quasielastic component the width of which saturates at a finite value for Q approaching zero, in contrast to the Q^2 -proportional dependence that we observe for water confined only in the direction normal to the ZrO_2 surface. Careful analysis of the translational diffusion of water in a fully hydrated Na-vermiculite, which, similar to the system we study, has a quasi-two-dimensional nature and exhibits the Q^2 -proportional dependence at low Q , yields a diffusion coefficient similar to that of bulk water, and a jump distance of 1.9 Å at 300 K.^{20,55} A large jump distance of 4.1 Å was obtained for quasi-two-dimensional translational water diffusion in purple membrane.^{10,11} It was proposed that the large jump length represented an average distance between neighboring potential minima of the diffusing molecule. For our system, similar argument suggests that the temperature-independent jump length we obtained corresponds to the distance between the potential minima of the diffusing free water molecule on the surface of the inner hydration layer.

Altogether, our findings suggest that the outermost layer of the surface water in ZrO_2 , the dynamics of which is assessable in a time-of-flight neutron experiment with 19 μeV resolution, shows little similarity to bulk water. It has lower molecular density, which makes long jumps possible, and its molecules form hydrogen bonds mostly with the immobile (on their time scale) water species of the inner hydration layer that are in direct contact with the hydroxylated surface. We observe a localized motion that can be described by a

rotational diffusion on a fast, picosecond time scale, and a much slower translational component of the diffusion. These two components are decoupled to a good approximation in the temperature range of 300–360 K. The localized component does not show a dramatic difference in correlation time with the hindered rotational motion in bulk water. In both bulk and surface water, the dynamics of the localized rotational component must be correlated with the typical hydrogen bond lifetime. The dynamics of the translational component slows down dramatically compared to bulk water. It is likely that the activation energy of 11.38 kJ/mol is related to the barrier separating the potential energy minima of the diffusing molecule. The translational diffusion of water molecules is no longer a complex cooperative process involving rearrangement of the neighboring water molecules with a non-Arrhenius behavior, but is a thermally activated, Arrhenius-type surface jump diffusion instead.

Finally, we want to emphasize that low density of molecular water in the hydration layers that leads to the dynamics very different from that of dense bulk water must be a direct consequence of the surface hydroxylation. There is an evidence that the density of surface water layers near Ag(111) electrode is similar to and even exceeds that of bulk water.^{56,57} In such systems with a dense network of hydrogen bonds, somewhat slower but still bulklike water dynamics can be expected. On the other hand, for oxide surfaces hydrated under ambient conditions one can expect the low density outermost water layers in contact with water molecules of the inner hydration layers to show the translational dynamics similar to that we observed for surface water in ZrO₂. Greater variations amongst oxides can be expected for the dynamics of the water molecules of the inner layer in direct contact with surface hydroxyl groups because of the higher sensitivity to the surface structure.

V. CONCLUSION

Our quasielastic neutron scattering study of surface water dynamics in ZrO₂ at and above room temperature has revealed a significant separation between the characteristic times for translational and rotational components of diffusion. The rotational correlation time demonstrates an Arrhenius-type behavior with the activation energy $E_A = 4.48$ kJ/mol, lower than $E_A = 7.74$ kJ/mol for bulk water.³³ The rotational diffusion takes place on picosecond time scale, and slows down by about a factor of 2 compared to bulk water at room temperature. In both systems, the dynamics of the localized rotational diffusion component must be correlated with the typical hydrogen bond lifetime. The translational diffusion, however, slows down by a factor of 40 at room temperature. Furthermore, the correlation time for translation diffusion exhibits an Arrhenius-type temperature dependence with the activation energy $E_A = 11.38$ kJ/mol, in a contrast to bulk water which is strongly non-Arrhenius at and below room temperature. Comparison of different models for jump diffusion processes suggests that water molecules, the dynamics of which can be probed in a time-of-flight neutron experiment with a 19 μ eV resolution, perform two-dimensional jumps at a well defined, almost temperature-independent distance of 4.21–4.32 Å.

Such a large jump distance cannot be reconciled with a bulk-water-like density of diffusing molecules. Instead, it is close to intermolecular distance of 4.66 Å in layers of water with the assumed density of 4.6 molecules per 100 Å², which is the known coverage of fully hydroxylated silica surface. Assuming the presence of about two hydration layers on top of the layer of surface OH groups, all having similar areal density of about 4.6 molecules per 100 Å², we obtain a good agreement with the weight loss water desorption measurements and the fraction of the elastic scattering observed in the experiment. Comparison with the much slower dynamics previously observed for a single layer of water on the hydroxylated surface of Cr₂O₃ (Ref. 24) further supports our hypothesis that we assess the dynamics of the outermost hydration layer, whereas slower motion of the water molecules in the inner hydration layer contributes to the elastic signal. In this scenario, the distance between the potential energy minima of the diffusing molecule on the surface of the inner hydration layer is the jump distance in a thermally activated, Arrhenius-type surface diffusion process. We propose that in oxides hydrated under ambient conditions the dynamics of the outermost water layer should be similar to surface water dynamics in ZrO₂.

ACKNOWLEDGMENTS

The author is thankful to D. Clough of Magnesium Elektron Inc. for providing the sample, to J. Gilman and R. Harris for assistance with the TGA measurements, and to S. Satija for the x-ray diffraction measurement. The author is indebted to J. Copley for assistance with data collection and valuable discussions and to R. Dimeo for assistance with the IDL programming code. The author benefited from the discussion with D. Price. The author is also grateful to C. Brown and D. Neumann for critical reading of the manuscript. Utilization of the DAVE package for the data analysis is acknowledged. This work utilized facilities supported in part by the National Science Foundation under Agreement No. DMR-0086210. Certain commercial materials and suppliers are identified in this paper to foster understanding. Such identification does not imply recommendation or endorsement by the National Institute of Standards and Technology, nor does it imply that the materials or suppliers identified are necessarily the best available for the purpose.

- ¹A. J. Dianoux, F. Volino, and H. Hervet, *Mol. Phys.* **30**, 1181 (1975).
- ²D. J. Cebula, R. K. Thomas, and J. W. White, *Clays Clay Miner.* **29**, 241 (1981).
- ³F. Volino, M. Pineri, A. J. Dianoux, and A. de Geyer, *J. Polym. Sci. A* **20**, 481 (1982).
- ⁴J. J. Tuck, P. L. Hall, M. H. B. Hayes, D. K. Ross, and C. Poinson, *J. Chem. Soc., Faraday Trans.* **80**, 309 (1984).
- ⁵C. Poinson, H. Estrade-Szwarczkopf, J. Conard, and A. J. Dianoux, *Physica B* **156–157**, 140 (1989).
- ⁶M.-C. Bellissent-Funel, J. Teixeira, K. F. Bradley, and S. H. Chen, *J. Phys. (Paris)* **2**, 995 (1992).
- ⁷M.-C. Bellissent-Funel, J. Teixeira, K. F. Bradley, S. H. Chen, and H. L. Crespi, *Physica B* **180–181**, 740 (1992).
- ⁸U. Wanderlingh, R. Giordano, and J. Teixeira, *J. Mol. Struct.* **296**, 271 (1993).
- ⁹M.-C. Bellissent-Funel, K. F. Bradley, S. H. Chen, J. Lal, and J. Teixeira, *Physica A* **201**, 277 (1993).

- ¹⁰R. E. Lechner, N. A. Dencher, J. Fitter, G. Buldt, and A. V. Belushkin, *Biophys. Chem.* **49**, 91 (1994).
- ¹¹R. E. Lechner, N. A. Dencher, J. Fitter, and T. Dippel, *Solid State Ionics* **70–71**, 296 (1994).
- ¹²M.-C. Bellissent-Funel, S. H. Chen, and J.-M. Zanotti, *Phys. Rev. E* **51**, 4558 (1985).
- ¹³M. Settles and W. Doster, *Faraday Discuss.* **103**, 269 (1996).
- ¹⁴M.-C. Bellissent-Funel, J.-M. Zanotti, and S. H. Chen, *Faraday Discuss.* **103**, 281 (1996).
- ¹⁵T. Takamuku, M. Yamagami, H. Wakita, Y. Masuda, and T. Yamaguchi, *J. Phys. Chem. B* **101**, 5730 (1997).
- ¹⁶S. Takahara, M. Nakano, S. Kittaka, Y. Kuroda, T. Mori, H. Hamano, and T. Yamaguchi, *J. Phys. Chem. B* **103**, 5814 (1999).
- ¹⁷J.-M. Zanotti, M.-C. Bellissent-Funel, and S. H. Chen, *Phys. Rev. E* **59**, 3084 (1999).
- ¹⁸S. Dellerue and M.-C. Bellissent-Funel, *Chem. Phys.* **258**, 315 (2000).
- ¹⁹M. Gay-Duchosal, D. Hugh Powell, R. E. Lechner, and B. Ruffe, *Physica B* **276–278**, 234 (2000).
- ²⁰J. Swenson, R. Bergman, and W. S. Howells, *J. Chem. Phys.* **113**, 2873 (2000).
- ²¹J. Swenson, R. Bergman, and S. Longeville, *J. Chem. Phys.* **115**, 11299 (2001).
- ²²E. Fratini, S. H. Chen, P. Baglioni, and M.-C. Bellissent-Funel, *Phys. Rev. E* **64**, 020201(R) (2001).
- ²³F. Mansour, R. M. Dimeo, and H. Peemoeller, *Phys. Rev. E* **66**, 041307 (2002).
- ²⁴Y. Kuroda, S. Kittaka, S. Takahara, T. Yamaguchi, and M.-C. Bellissent-Funel, *J. Phys. Chem. B* **103**, 11064 (1999).
- ²⁵M. Y. He and J. G. Ekerdt, *J. Catal.* **87**, 238 (1984); **87**, 381 (1984); **90**, 17 (1984); N. B. Jackson and J. G. Ekerdt, *ibid.* **101**, 90 (1986); S. C. Tseng, N. B. Jackson, and J. G. Ekerdt, *ibid.* **109**, 284 (1988); N. B. Jackson and J. G. Ekerdt, *ibid.* **126**, 31 (1990); **126**, 46 (1990); R. G. Silver, C. J. Hou, and J. G. Ekerdt, *ibid.* **118**, 400 (1989).
- ²⁶C.-K. Loong, J. W. Richardson, and M. Ozawa, *J. Catal.* **157**, 636 (1995).
- ²⁷S. H. Chen, C. Liao, F. Sciortino, P. Gallo, and P. Tartaglia, *Phys. Rev. E* **59**, 6708 (1999).
- ²⁸A. Faraone, L. Liu, and S. H. Chen, *J. Chem. Phys.* **119**, 6302 (2003).
- ²⁹G. Gerrato, S. Bordiga, S. Barbera, and C. Morterra, *Surf. Sci.* **377–379**, 50 (1997).
- ³⁰M. R. Alvarez and M. J. Torralvo, *Colloids Surf., A* **83**, 175 (1994).
- ³¹M. R. Alvarez, M. J. Torralvo, Y. Grillet, F. Rouquerol, and J. Rouquerol, *Stud. Surf. Sci. Catal.* **87**, 293 (1994).
- ³²S. H. Chen, J. Teixeira, and R. Nicklow, *Phys. Rev. A* **26**, 3477 (1982).
- ³³J. Teixeira, M.-C. Bellissent-Funel, S. H. Chen, and A. J. Dianoux, *Phys. Rev. A* **31**, 1913 (1985).
- ³⁴M. Daturi, E. Finocchio, C. Binet, J.-C. Lavalley, F. Fally, and V. Perrichon, *J. Phys. Chem. B* **103**, 4884 (1999).
- ³⁵A. Badri, C. Binet, and J. C. Lavalley, *J. Chem. Soc., Faraday Trans.* **92**, 4669 (1996).
- ³⁶H. Knözinger, in *The Hydrogen Bond—Recent Developments in Theory and Experiments*, edited by P. Schuster, G. Zundel, and C. Sandorfy (North-Holland, Amsterdam, 1976), p. 1263.
- ³⁷J. R. D. Copley and J. C. Cook, *Chem. Phys.* **292**, 477 (2003).
- ³⁸V. F. Sears, *Can. J. Phys.* **44**, 1299 (1966); **45**, 237 (1966).
- ³⁹P. A. Egelstaff, *An Introduction to the Liquid State* (Academic, London, 1967).
- ⁴⁰P. L. Hall and D. K. Ross, *Mol. Phys.* **42**, 673 (1981).
- ⁴¹K. S. Singwi and A. Sjölander, *Phys. Rev.* **119**, 863 (1960).
- ⁴²I. Rosciszewski, *Acta Phys. Pol. A* **41**, 549 (1972).
- ⁴³R. Stockmeyer, *Ber. Bunsenges. Phys. Chem.* **80**, 625 (1976).
- ⁴⁴A. Renouprez, P. Fouilloux, R. Stockmeyer, H. M. Conrad, and G. Goeltz, *Ber. Bunsenges. Phys. Chem.* **81**, 429 (1977).
- ⁴⁵J. P. Coulomb, M. Bienfait, and P. Thorel, *J. Phys.* **42**, 293 (1981).
- ⁴⁶M. Bienfait, *Europhys. Lett.* **4**, 79 (1987).
- ⁴⁷K. W. Herwig, Z. Wu, P. Dai, H. Taub, and F. Y. Hansen, *J. Phys. Chem.* **107**, 5186 (1997).
- ⁴⁸M. Bienfait, B. Asmussen, M. Johnson, and P. Zeppenfeld, *Surf. Sci.* **460**, 243 (2000).
- ⁴⁹R. E. Lechner, *Solid State Ionics* **77**, 280 (1995).
- ⁵⁰M. Bienfait, J. P. Coulomb, and J. P. Palmari, *Surf. Sci.* **182**, 557 (1987); **185**, 352 (1987); **241**, 454 (1991).
- ⁵¹J. Teixeira, M.-C. Bellissent-Funel, and S. H. Chen, *J. Phys.: Condens. Matter* **2**, SA105 (1990).
- ⁵²M. G. Sceats, M. Stavola, and S. A. Rice, *J. Chem. Phys.* **70**, 3927 (1979).
- ⁵³D. M. Lyons, J. P. McGrath, and M. A. Morris, *J. Phys. Chem. B* **107**, 4607 (2003).
- ⁵⁴R. Mills, *J. Phys. Chem.* **77**, 685 (1973).
- ⁵⁵E. Mamontov, *J. Chem. Phys.* (in press).
- ⁵⁶M. F. Toney, J. N. Howard, J. Richer *et al.*, *Nature (London)* **368**, 444 (1994).
- ⁵⁷M. F. Toney, J. N. Howard, J. Richer *et al.*, *Surf. Sci.* **335**, 326 (1995).